p31^{comet} acts to ensure timely spindle checkpoint silencing subsequent to kinetochore attachment

Robert S. Hagan[1,2,5], Michael S. Manak[2,3], Håkon Kirkeby Buch[2,3,6], Michelle G. Meier[4], Patrick Meraldi[1,4], Jagesh V. Shah[2,3*] and Peter K. Sorger[1,2*]

*Co-corresponding authors

[1]Center for Cell Decision Processes, [2]Department of Systems Biology, Harvard Medical School, MA 02115

[3]Renal Division, Brigham and Women's Hospital, Boston, MA 02115

[4]Institute of Biochemistry, Eidgenössische Technische Hochschule (ETH) Zurich, CH-8093 Zurich, Switzerland

[5]Division of Pulmonary and Critical Care Medicine, Johns Hopkins University School of Medicine, Baltimore, MD 21205

[6]Current address: Institute of Cell Biology, Eidgenössische Technische Hochschule (ETH) Zurich, CH-8093 Zurich, Switzerland

*Please address correspondence to:

Peter K. Sorger
Harvard Medical School
200 Longwood Avenue
WAB Room 438
Boston MA 02115
617-432-6901/6902
peter_sorger@hms.harvard.edu
cc: christopher_bird@hms.harvard.edu

Jagesh V. Shah (designate)
Harvard Medical School
4 Blackfan Circle
HIM Room 564
Boston, MA 02115
617-525-5912/5965
jagesh_shah@hms.harvard.edu

Running title: p31 ensures timely checkpoint silencing

Keywords: spindle checkpoint, p31^{comet}, Mad2, checkpoint silencing, mitotic timing

Characters (w/o M&M, refs or abstract): 30116 characters without spaces

HIGHLIGHT SUMMARY

p31^{comet} opposes the activities of the Mad2 spindle assembly checkpoint protein, localizes to unattached kinetochores and, like many checkpoint proteins, turns over rapidly at that site. Depletion of p31^{comet} prevents timely passage into anaphase showing that mitotic progression requires an active mechanism for silencing the spindle checkpoint. (309 characters)

ABSTRACT

The spindle assembly checkpoint links the onset of anaphase to completion of chromosome-microtubule attachment and is mediated by the binding of Mad and Bub proteins to kinetochores of unattached or maloriented chromosomes. Mad2 and BubR1 traffic between kinetochores and the cytosol, thereby transmitting a "wait anaphase" signal to the anaphase-promoting complex. It is generally assumed that this signal dissipates automatically upon kinetochore-MT binding but it has been shown that under conditions of nocodazole-induced arrest p31^{comet}, a Mad2-binding protein, is required for mitotic progression. In this paper we investigate the localization and function of p31^{comet} during normal, unperturbed mitosis in human and marsupial cells. We find that, like Mad2, p31^{comet} traffics on and off kinetochores and is also present in the cytosol. Cells depleted of p31^{comet} arrest in metaphase with mature bipolar kinetochore-microtubule attachments, a satisfied checkpoint and high cyclin B levels. Thus, p31^{comet} is required for timely mitotic exit. We propose that p31^{comet} is an essential component of the machinery that silences the checkpoint during each cell cycle. (169 words)

INTRODUCTION

The spindle assembly checkpoint prevents errors in chromosome segregation by linking the dissolution of sister chromatid cohesion to the formation of bipolar kinetochore-microtubule attachments (for review see (Musacchio and Salmon, 2007)). The Mad, Bub, and Mps1 components of the checkpoint were first isolated in *S. cerevisiae* and are highly conserved among eukaryotes (Hoyt *et al.*, 1991; Li and Murray, 1991; Hardwick *et al.*, 1996). During prometaphase and metaphase, binding of spindle checkpoint proteins to unattached or maloriented kinetochores initiates a signaling cascade that inhibits Cdc20, an essential activator of the anaphase promoting complex/cyclosome (APC/C). The APC/C is an E3 ubiquitin ligase whose targets include cyclin B, securin, and other proteins whose degradation is necessary for cells to transition from metaphase to anaphase. Mad2 and BubR1 associate with each other in a large mitotic checkpoint complex (MCC) that also contains Cdc20 and Bub3 (Hardwick *et al.*, 2000; Sudakin *et al.*, 2001). Rapid shuttling of Mad2, BubR1, and Cdc20 between kinetochores and the cytosolic MCC complex (Kallio *et al.*, 2002; Howell *et al.*, 2004; Shah *et al.*, 2004), is thought to transmit the "wait anaphase" signal that links the state of kinetochore attachment to APC/C activity (Ciliberto and Shah, 2009; Kulukian *et al.*, 2009). The precise nature of this signal remains unclear, but structural and biochemical data point to a switch between open and closed conformations of Mad2 (Luo *et al.*, 2004; De Antoni *et al.*, 2005): Mad2 is closed (C-Mad2) when bound to Mad1 at kinetochores or to Cdc20. Transient dimerization between C-Mad2 and an open, cytosolic Mad2 conformation (O-Mad2) is thought to promote binding to and inhibition of Cdc20 (Mapelli *et al.*, 2007; Yang *et al.*, 2008; Simonetta *et al.*, 2009). Mad2 and BubR1 also appear to have a kinetochore-independent role in regulating APC/C early in mitosis prior to the establishment of an active spindle checkpoint in early prometaphase (Meraldi *et al.*, 2004).

The spindle checkpoint is traditionally regarded as a negative regulator of mitotic exit with Mad2 playing a particularly direct role in inhibiting proteins that regulate anaphase onset. Much less is known about processes that silence the checkpoint, activate APC/C, and promote mitotic progression when all

chromosomes are correctly spindle-bound (Ciliberto and Shah, 2009). Historically, it has been assumed that spontaneous decay of an inhibitory checkpoint signal is involved. However, recent work has posited a role for the E2 ubiquitin ligase UbcH10 in disassembling the MCC-APC/C complex via ubiquitination of Cdc20 (Reddy *et al.*, 2007) and consequent formation of active APC/C. In vitro biochemical studies have also implicated p31^{comet} in the dissociation of anaphase-inhibitory complexes (Reddy *et al.*, 2007; Teichner *et al.*, 2011). Consistent with this view, RNAi-mediated depletion of p31^{comet}, a protein that binds C-Mad2 (Habu *et al.*, 2002; Xia *et al.*, 2004; Mapelli *et al.*, 2006; Yang *et al.*, 2007), reduces the rate at which cells recover from nocodazole-induced mitotic arrest (Xia *et al.*, 2004). As such, a role of p31^{comet} in exit from an unperturbed mitosis has not yet been studied. The distinction between nocodazole-induced mitotic arrest and normal mitotic progression is important: recent work has demonstrated that Ube2S, an E2 involved in ubiquitin chain extension, behaves differently in nocodazole-arrested cells versus normally growing cells (Garnett *et al.*, 2009). It is an open question as to whether p31comet behaves in this way. Here we examine these questions by combining RNAi-mediated protein depletion of p31^{comet} and other checkpoint proteins, live-cell imaging and quantitative modeling. We find that p31^{comet} binds to unattached kinetochores in mitosis in a Mad2-dependent manner, that this binding is highly dynamic, and that p31^{comet} is essential in every cell cycle for rapid inactivation of the spindle checkpoint and for timely passage from metaphase into anaphase. Thus, mitotic progression requires an active mechanism for silencing the spindle checkpoint.

RESULTS

p31^{comet} is required for mitotic exit in each cell cycle

The time of anaphase onset relative to nuclear breakdown (NBD; defined as T=0) was determined by live-cell imaging of HeLa cells stably expressing mRFP or EGFP fusions to Histone2B. In unperturbed HeLa cells anaphase onset times have a characteristic skew-normal distribution with a modal (peak) value of (T=) 26 ± 1.5 min (Meraldi *et al.*, 2004) and very few cells (~5%) entering anaphase prior to 18 min. In contrast, when cells were depleted of Mad2 (Figure 1C), ~90% entered

anaphase prematurely (before 18 minutes, see figure 1A). Premature anaphase onset was phenocopied by over-expression of GFP-tagged p31^{comet}: >80% of cells transiently expressing GFP-p31^{comet} from a CMV promoter entered anaphase prematurely (Fig 1A;(Yang *et al.*, 2007)).

Very few unperturbed HeLa cells were still in metaphase at t=45 min (~5%). However, when cells were depleted of p31^{comet} by RNAi (Figure 1C and Supplemental Figure 1) we observed that ~95% were in metaphase at 45 min as compared to 10% of control RNAi treated cells (Figure 1B; the difference between 5% and 10% is presumed to represent the nonspecific effects of siRNA transfection). This phenotype resembled that of transient over-expression GFP-Mad2 (~60% mitotic; Figure 1B) or nocodazole exposure (>95% mitotic (Meraldi *et al.*, 2004) both of which are known to arrest cells in metaphase (Sotillo *et al.*, 2007). Some over-expression or depletion phenotypes for p31^{comet} have been described previously but direct comparison with phenotypes associated with changes in Mad2 levels makes the pattern of opposing effects clear: over-expression of p31^{comet} or depletion of Mad2 causes premature mitotic exit whereas depletion of p31^{comet} or over-expression of Mad2 causes mitotic arrest. Mad2 is well known as an anaphase inhibitory factor and p31^{comet} therefore acts as an anaphase promoting factor.

Why did cells depleted of p31^{comet} arrest in mitosis? Immunofluorescence revealed that p31^{comet} depleted cells had congressed chromosomes, high levels of cyclin B and low levels of cyclin A (Figure 2A). To determine whether chromosomes were bound correctly to MTs, cells we assayed for inter-kinetochore stretching and for the levels of Mad2 and Bub proteins. Following chromosome congression, bipolar attachment of spindle MTs to paired sisters creates pulling forces that can be assayed by measuring distances between puncta of core kinetochore proteins (Shelby *et al.*, 1996). Using a recently developed kinetochore-tracking assay and HeLa cells that express the centromeric histone CENP-A (Jaqaman *et al.*, 2010), we found that sister centromeres in metaphase cells depleted of p31^{comet} were highly stretched and that they had therefore achieved bipolar attachment. If anything, inter-kinetochore distances were higher in p31^{comet}-depleted than in control cells (1.13 ± 0.23 μm versus

1.01 ± 0.25 μm, representing the mean and standard deviation of > 240 kinetochore pairs for each condition; Figure 2B). We conclude that kinetochore-microtubule attachment is normal in the absence of p31^{comet} and that spindles can generate normal pulling forces. As a further assay for correct spindle assembly we asked whether the spindle assembly checkpoint was activated as assayed by measuring the levels of kinetochore-bound Mad and Bub proteins. In normal mitosis checkpoint proteins are enriched on prometaphase kinetochores but then dissociate as spindle microtubules bind to kinetochores during metaphase (Hoffman *et al.*, 2001). When Mad1, Mad2, Bub1, and BubR1 staining was compared in p31^{comet}-depleted and control cells using immunofluorescence microscopy, levels of kinetochore-bound checkpoint proteins were indistinguishable (Figure 2C). Mad1 and Mad2 levels, when compared relative to CREST were undetectable in metaphase cells treated with control or p31^{comet} RNAi (Supplemental Figure 2). Similar results were observed for checkpoint proteins Mps1 and Bub3 and for CENP-E and CENP-F (Supplemental Figure 3). Depleting p31^{comet} does not interfere with chromosome-MT attachment nor does it prevent normal dissociation of checkpoint proteins from kinetochores as mitosis proceeds. Thus, p31^{comet} loss arrests cells subsequent to kinetochore-MT attachment at a point in the cell cycle that is distinct from a checkpoint-mediated arrest.

Binding of p31^{comet} to kinetochores

To determine the subcellular localization of p31^{comet}, cells were co-stained with affinity-purified anti-p31^{comet} antibodies and anti-centromere/kinetochore (CREST) serum (Figure 3A, Supplemental Figure 1). p31^{comet} was found at high levels on unattached kinetochores in prometaphase, at significantly lower levels as kinetochores became MT-bound during metaphase and in the cytosol at all cell-cycle stages. Both kinetochore and cytosolic staining by anti-p31^{comet} antibodies were specific insofar as they were reduced significantly by RNAi directed against p31^{comet} (Figure 3B and 3C, Supplemental Figure 1) and the pattern was identical to those of Mad1 and Mad2 (Chen *et al.*, 1998; Howell *et al.*, 2004; Shah *et al.*, 2004); these data confirm and extend previous observations from Habu

et al (Habu *et al.*, 2002). RNAi-mediated depletion of Mad2 reduced levels of p31^{comet} staining on prometaphase kinetochores to the same extent as depletion of p31^{comet} itself (>10-fold; Figures 3B and 3C). p31^{comet} is therefore among the few proteins known whose binding to kinetochores is completely dependent on the presence of Mad2 (Vigneron *et al.*, 2004).

To observe the precise dynamics of p31^{comet} localization we generated PtK2 cells that stably expressed an EYFP fusion to the human protein. Live-cell analysis of these cells confirmed localization data obtained from immunostained HeLa cells: p31^{comet}-EYFP was present on unattached kinetochores in early prophase/prometaphase and then lost as kinetochores became MT-bound (Figure 3C, arrows and Supplemental Movie #1). Cells entered anaphase only after levels of kinetochore-associated p31^{comet}-EYFP had fallen below the level of detection (Figure 3B), a behavior similar to what has previously been observed for both Mad1 and Mad2. As PtK2 cells progressed into late metaphase and kinetochores became MT-bound, p31^{comet}-EYFP was observed to accumulate at spindle poles and to remain there until late anaphase, at which point it dissociated and fluorescence was lost (Figure 3D, short arrowheads). In HeLa cells, anti-p31^{comet} antibodies did not appreciably stain spindle poles. However, it has previously been established that whereas Mad2 localizes to spindle poles late in mitosis in PtK2 it does not in HeLa cells (Howell *et al.*, 2000; Shah *et al.*, 2004). Thus, whatever the origins of differential spindle staining between PtK2 and Hela cells, similar results have been obtained with Mad2 and p31^{comet}: levels of Mad2 and p31^{comet} on individual kinetochores were highly correlated in both cell types.

Kinetochore dependent and independent p31^{comet} functions

The fact that RNAi and over-expression phenotypes of Mad2 and p31^{comet} are mirror images of each other and that localization of p31^{comet} to kinetochores requires Mad2 raises the question whether the arrest of p31^{comet}-depleted cells is Mad2-dependent. In co-transfection experiments we observed that whereas 70 ±20% of p31^{comet}-depleted cells (co-transfected with second control siRNA) were in mitosis

45 minutes after NBD, only 12±4% of cells depleted of both Mad2 and p31^{comet} were similarly arrested (Figure 4A). Co-depletion phenotypes were slightly weaker than single-depletion phenotypes (e.g. with Mad2 RNAi alone, no cells were in mitosis at 45 minutes) presumably due to competition between co-transfected siRNA oligos. Even so, we conclude that the arrest of cells following depletion of p31^{comet} requires Mad2.

To determine which other components of the checkpoint are involved in the mitotic arrest caused by loss of p31^{comet}, we co-depleted p31^{comet} with Mad1 and Nuf2R. Mad1 is a checkpoint protein that binds to and recruits Mad2 to kinetochores (Chen *et al.*, 1998) and Nuf2R is a structural component of kinetochores required for kinetochore binding by Mad1, Mad2 and other checkpoint proteins (DeLuca *et al.*, 2003). Single depletion of Mad1 (4±3% mitotic cells at t=45 min) or Nuf2R (10±4% mitotic cells) inactivated the checkpoint, as described previously (Meraldi *et al.*, 2004; McAinsh *et al.*, 2006). However, the mitotic arrest caused by p31^{comet} depletion was not overcome by co-depletion with either Mad1 (87±18% mitotic cells) or Nuf2R (77±7% mitotic cells). Thus, even though depletion of Mad1, Mad2 or Nuf2 abrogates the checkpoint, mitotic arrest caused by loss of p31^{comet} is overcome only by Mad2 depletion (Figure 4A). Because depletion of either Mad1 or Nuf2 causes Mad2 to dissociate from kinetochores, our data also suggest that p31^{comet} is also acting via cytosolic Mad2, a fraction of which is associated with the MCC. The results also serve as further evidence that p31^{comet} depletion does not simply arrest cells in a checkpoint-dependent manner.

Cumulative frequency graphs that capture the timing of mitotic exit in single cells provide a kinetic picture of cell cycle progression and a more nuanced view of function. We observed that half of all cells transfected with control RNAi progressed from NBD to anaphase at 21 minutes (the modal time), in line with previous data (Figure 4B and 4C). The modal time of anaphase entry was not affected by Mad1 depletion, but depletion of Mad2 cut the time in half, to ~12 min, consistent with previous data showing that Mad2 but not Mad1 is involved in the timing of mitotic exit independent of checkpoint control (Meraldi *et al.*, 2004). Kinetic analysis also revealed that cells depleted of p31^{comet} do not arrest

permanently in metaphase but instead proceed very slowly into anaphase such that roughly 40% had exited mitosis by t=180min (Figure 4B and C, orange line). This contrasts with the phenotype of a classical checkpoint arrest provoked by depletion of essential spindle components in which cells enter a near-complete arrest of 6 or more hours in duration (Meraldi *et al.*, 2004). As mentioned above, Mad2 depletion was epistatic to p31^{comet} depletion and co-depletion phenocopied the kinetics of Mad2 depletion alone ($t_{1/2}$ ~11 min, Figure 4B; purple line). In contrast, co-depleting cells of Mad1 and p31^{comet} resulted in a phenotype midway between control RNAi or p31^{comet}-depletion alone, causing cells to exit mitosis with a $t_{1/2}$ ~ 90 min (Figure 4C; brown line). While the intermediate phenotype could be due to incomplete Mad1 knockdown, we would expect at least a subset of cells would show a faster mitotic transit if in fact p31^{comet} is downstream of Mad1. Instead, we interpret this intermediate phenotype as reflecting a role for p31^{comet} in antagonizing both the kinetochore-dependent Mad2 functions (this manifests itself as the difference between the depletion phenotypes for p31^{comet} alone versus p31^{comet} in combination with Mad1 or Nuf2) and the kinetochore-independent functions of Mad2 (this manifests itself as the difference between the double depletion phenotypes for p31^{comet} and Mad1 or Nuf2 versus p31^{comet} and Mad2).

Two pools of Mad2 are found on kinetochores: a rapidly cycling pool of Mad2 that transiently associates with a stable pool of Mad2 that is tightly bound to Mad1 (Shah *et al.*, 2004). To assay the rate of turnover of p31^{comet} on kinetochores we performed fluorescence recovery after photobleaching experiments (FRAP) on PtK2 cells stably expressing p31^{comet}-EYFP. Figure 5 (panel A) illustrates a representative FRAP sequence in which one of a pair of unattached kinetochores is rapidly bleached and its recovery observed. In unperturbed mitoses the mean half-recovery time of p31^{comet}-EYFP at unattached kinetochores was 10 ± 0.9 sec (SEM, n=26 kinetochores from 15 cells) with a total percentage recovery of 79 ± 3% (SEM). In cells arrested with nocodazole (300 nM), the mean half-recovery time was 12 ±1.3 s (SEM, n=11 kinetochores from 10 cells) with a total percentage recovery of 81 ± 5 % (SEM), values that are indistinguishable from normal prometaphase kinetochores. These

recovery kinetics are similar to those for the rapidly exchanging pool of Mad2 ($t_{1/2}$=10.8±1.2 s) (Shah *et al.*, 2004). To determine the rate of dissociation of p31^{comet} from a pool of Mad2 that is not dynamic, we examined the interphase nuclear envelope, which carries stable Mad1-Mad2 complexes (Shah *et al.*, 2004). The fraction of p31^{comet} bound to the nuclear envelope was observed to dissociate at a relatively slow rate ($t_{1/2}$ = 56 ± 12s SEM, R% = 67.1 ± 2.46 %, n = 13 cells, Figures 5D and 5E) consistent with tight binding of C-Mad2 to Mad1. In contrast, the nucleoplasmic fraction of p31^{comet} exhibited a mean half-recovery time of 0.53s ± 0.36s (SEM) with a percent recovery of 32.9 % ± 2.46% (SEM), consistent with a very rapid diffusible nucleoplasmic pool of p31^{comet}. Thus, p31^{comet} traffics on and off kinetochores at nearly the same rate as the dynamic pool of Mad2. Moreover, rapid association-dissociation of p31^{comet} from a Mad1-Mad2 scaffold is a special property of kinetochores, because Mad1-Mad2 complexes on the nuclear envelope bind relatively stably to p31^{comet}.

DISCUSSION

Activation of the spindle assembly checkpoint by unattached kinetochores in normally dividing cells and by maloriented kinetochores (particularly those generated by spindle poisons) has been widely studied in higher and lower eukaryotes but the mechanisms that extinguish checkpoint signaling at the end of metaphase are less well understood (Ciliberto and Shah, 2009). Historically, it has been assumed that the SAC comprises only negative regulators of mitotic progression, However, data showing delayed recovery of p31^{comet}-depleted cells from nocodazole-mediated arrest (Xia *et al.*, 2004) and in vitro studies of p31^{comet} binding proteins (Reddy *et al.*, 2007; Teichner *et al.*, 2011) have highlighted a role for p31^{comet} in APC/C activation and mitotic progression. The ubiquitin conjugating enzymes UbcH10 (Reddy *et al.*, 2007) and Ube2S (Garnett *et al.*, 2009; Williamson *et al.*, 2009; Wu *et al.*, 2010) have also been implicated in silencing the spindle assembly checkpoint. In this paper we examine the role of p31^{comet} in cells that have not been exposed to spindle poisons. We find that RNAi-mediated depletion of p31^{comet} dramatically slows the entry of cells into anaphase, showing that p31^{comet} is required in each cell

cycle for timely mitotic exit. Although arrest is not absolute, the phenotype is strong with ~80% of p31^{comet} depleted cells still in metaphase 3 hours after nuclear envelope breakdown as compared to progression of 100% of cells within 30 min under normal circumstances.

A remarkable feature of forced changes in Mad2 and p31^{comet} levels is that the resulting phenotypes are mirror images of each other: over-expression of Mad2 or depletion of p31^{comet} blocks or dramatically slows mitosis whereas depletion of Mad2 or over-expression of p31^{comet} causes rapid progression into anaphase. In p31^{comet} depleted cells sister chromatids have achieved normal bipolar attachment and SAC proteins including Mad2 have dissociated from kinetochores, showing that checkpoint conditions have been satisfied at kinetochores. Our findings suggest that p31^{comet} is a cytoplasmic checkpoint activator required for mitotic progression after the loss of checkpoint proteins from kinetochores.

Early in mitosis, prior to the completion of chromosome-MT attachment, we find that p31^{comet} is similar to Mad2 and other checkpoint proteins in localizing to kinetochores. Previous work by Habu and colleagues (Habu *et al.*, 2002) demonstrated p31^{comet} localization to a chromatin domain roughly coincident with centromeres; using new p31^{comet} antibodies and a GFP fusion protein we show that puncta of p31^{comet} co-localize with core kinetochore proteins. Kinetochore localization by p31^{comet} is Mad2-dependent and is lost when chromosomes bind spindle MTs. The recruitment of Mad2 to kinetochores is a complex process thought to play an integral role in generation of the "wait-anaphase" signal. Mad2 in the closed conformation is bound directly to Mad1 and serves as a template for conversion of open O-Mad2 into its active and closed C-Mad2 form after which it dissociates and binds to Cdc20 in the cytosol, thereby blocking APC/C activity (Xia *et al.*, 2004; Mapelli *et al.*, 2006; Simonetta *et al.*, 2009). The conversion of O-Mad2 into C-Mad2 at unattached kinetochores results in association and dissociation of a pool of Mad2 from the stable Mad2-Mad1 oligomer with a half-life ~11 sec (as measured by FRAP) (Shah *et al.*, 2004). It has been estimated that this permits ~60 molecules of C-Mad2 to be generated per detached kinetochore per second (Ciliberto and Shah, 2009). Remarkably,

we find that p31^{comet} traffics through the kinetochore with kinetics indistinguishable from that of Mad2 (FRAP recovery $t_{1/2}$ ~11 sec) implying similarly rapid association and dissociation kinetics. This observation argues against the simplest model for p31^{comet} function, namely that it extinguishes the wait anaphase signal by acting as a stable cap on Mad1/C-Mad2 complexes that functions by blocking binding to and activation of O-Mad2 (Mapelli *et al.*, 2006). The capping model found initial support from the observation that p31^{comet} has ~40-fold greater affinity for C-Mad2 than O-Mad2 (Vink *et al.*, 2006). Indeed, we find that p31^{comet} binds Mad1/C-Mad2 complexes present on the interphase nuclear envelope and that turnover is slow (FRAP recovery $t_{1/2}$ ~60 sec,) like the turnover of stable Mad1/C-Mad2 association themselves (Shah *et al.*, 2004). The function of the interphase Mad1/C-Mad2 complex is not known but its ability to stably bind p31^{comet} argues that avid p31^{comet} -C-Mad2 association can occur in vivo. The binding of p31^{comet} to unattached kinetochores therefore, appears to be considerably weaker than binding to the nuclear envelope, implying either that p31^{comet} or Mad2 are modified in some way or that it is stable Mad2-p31^{comet} complexes that traffic on and off kinetochores.

We have previously demonstrated that the consequences of dissociating Mad2 from kinetochores, for example by depleting cells of Mad1or the kinetochore structural component Nuf2, is distinct from the phenotype of depleting Mad2. In all three cases SAC function is inactivated but the cytosolic Mad2 present in Mad1 or Nuf2-depeleted cells has a role in ensuring the correct timing of mitosis that is functionally (if not necessarily biochemically) distinct from its role in sensing the presence of maloriented chromosomes. It is presumed that this function involves the MCC complex. In this paper we show that co-depletion of p31^{comet} and Mad2 phenocopies Mad2 depletion alone: cells enter anaphase so rapidly ($t_{1/2}$ for NEBD to anaphase ~ 12min) as to indicate that both the SAC and timing functions of Mad2 are abrogated. However, the situation is different following co-depletion of p31^{comet} and either Mad1 or Nuf2. In these cases we observe an intermediate phenotype with cells slowly exiting mitosis over the course of ~3 hr. This implies a function for p31^{comet} as a regulator of the cytosolic Mad2 present in the MCC. Kinetochores are unable to generate active Mad2 in the absence of

Mad1 or Nuf2 and we presume that this is also the case in doubly depleted p31^{comet}/Mad1 or p31^{comet} /Nuf2 cells. However, a relatively small pool of active Mad2 is present at the start of mitosis and forms the MCC timer (Sudakin *et al.*, 2001; Meraldi *et al.*, 2004). We speculate that in the absence of p31^{comet} the timer portion of C-Mad2 is only slowly extinguished and the transition into anaphase is therefore delayed. When the checkpoint is able to function normally then much more C-Mad2 can be generated and the consequences of p31^{comet} depletion are correspondingly more severe. In the absence of Mad2 itself, no inhibitor to mitotic progression is generated and the combined p31^{comet}/Mad2 depletion phenocopies Mad2 depletion.

To begin to develop a quantitative understanding of p31^{comet} activities we created a simple (toy) computational model of checkpoint signaling. This model includes several competing processes whose rates have been estimated experimentally (see Methods) including: (i) kinetochore generation of C-Mad2 from a kinetochore scaffold (K-C-Mad2), (ii) interaction of C-Mad2 with APC/C (or MCC-APC/C), (iii) generation of C-Mad2 from a cytoplasmic pool of C-Mad2, a potential amplification process (Simonetta *et al.*, 2009), (iv) binding of p31^{comet} to C-Mad2 so as to block subsequent binding and conversion of O-Mad2 and to potentiate the dissociation of C-Mad2-APC/C complexes(Reddy *et al.*, 2007; Teichner *et al.*, 2011).

When p31^{comet} levels were varied in simulation from 0-120 nM (endogenous levels are estimated to be ~100 nM based on calibrated Western blots) and steady-state levels of APC/C plotted, we observed two regimes: when [p31^{comet}]< 60 nM active APC/C levels were low and the checkpoint chronically active, as expected, whereas with [p31^{comet}]> 90 nM APC/C was chronically active and the checkpoint was bypassed, a state that mimics p31^{comet} overexpression in cells (Figure 6A). Similar behavior was observed when kinetochore-dependent reactions were turned off, mimicking the consequences of kinetochore-MT attachment and checkpoint silencing (Figure 6B). Simulation of [p31^{comet}] <60nM in the absence of checkpoint-active kinetochores mimics the strong block to mitotic progression observed following RNAi of p31^{comet} whereas checkpoint resolution was observed at

[p31^{comet}] >80nM in the absence of active kinetochores. The strong dependence of APC/C activity on p31^{comet} levels shows that robust regulation can be achieved if we postulate a modest two-fold rise in p31^{comet} between early and late mitosis (Figure 6C). However, there is no evidence that total p31^{comet} levels change through mitosis, and we therefore speculate that a change in protein activity is involved (this is modeled by changing active p31^{comet} from 50nM, dashed lines, to 100 nM, sold lines). With a two-fold increase in the concentration or activity of active p31^{comet} we observe a two-fold increase in the concentration of capped, kinetochore-localized C-Mad2 (p31-K-C-Mad2 in Figure 6C). In addition, a dynamic equilibrium between two inhibited APC/C species: C-Mad2:APC/C and p31:C-Mad2:APC/C at [active p31^{comet}]= 50nM is replaced by the rapid decay of inhibited APC/C at [active p31^{comet}]= 100nM and formation of functional APC/C. Our admittedly simple simulations therefore integrate a number of biochemical processes to suggest that both of the postulated functions of p31^{comet} are important to its biological function: blocking the conversion of O-Mad2 to C-Mad2 (Vink *et al.*, 2006) and promoting the dissociation of the inhibited MCC-APC/C complex(Reddy *et al.*, 2007; Teichner *et al.*, 2011).

Based on available experimental data and the results of quantitative simulations we propose a model whereby p31^{comet} affinity for Mad2 is low, and therefore inhibitor dissociation is reduced, during active checkpoint signaling but that once kinetochores attach, p31^{comet} avidly binds Mad2 resulting in the increased activity of inhibitor dissociation. At a threshold level of activity, which need only be <2-fold greater than at the start of mitosis, p31^{comet} is able to overwhelm all active C-Mad2-generating mechanisms and dissociate all inhibited APC/C. Since we have shown that p31^{comet} actively traffics through kinetochores early in mitosis, it is appealing to propose that trafficking is associated with p31^{comet} regulation. p31^{comet} and Mad2 are quite similar in structure (Yang *et al.*, 2007) making conformational regulation of p31^{comet} a possibility, with post-translational modification (perhaps by a checkpoint kinase) an obvious alternative.

MATERIALS AND METHODS

Generation of plasmids and cell lines

Mad2 (EST Genbank ID R10991) was subcloned by PCR into pGEX-6P-2 (Amersham Biosciences**)** and pEGFPC1 (Clontech). p31^{comet} (IMAGE clone 321778, ATCC) was subcloned into pEGFPC1 and pFBnHis10HA. The cDNA for mRFP, a kind gift of R. Tsien, was fused to histone H2B in pCDNA3.1 (Invitrogen). All plasmids were confirmed by sequencing. Human p31^{comet} cDNA was amplified from a HeLa cDNA library with EcoRI and BamHI restriction sites by standard methods and the following primers: (5'-atgcatgcat**GAATTC**ATGGCGGCGCCGGAGGCGGAG-3' and 5'-atgcatgcat**GGATCC**CTCGCGGAAGCCTTTAAATGT-3'). This EcoRI-BamHI PCR product was ligated into the C2 and N3-frames of the Clontech EYFP plasmid to produce both N-terminal and C-terminal fusion cDNAs, respectively. PtK2 cells stably expressing EYFP fusions to human p31comet were generated via retroviral transduction as previously described (Shah *et al.*, 2004). PtK2 cell lines were maintained in CO2-dependent culture medium and switched to a Leibovitz L-15-based HEPES-buffered medium for live imaging (Shah *et al.*, 2004).

Cell culture,antibodies, and immunoblotting

HeLa, Histone 2B-GFP HeLa , HeLa Histone 2B-mRFP, and HeLa EGFP-CENP-A cells were generated and cultured as described (Meraldi et al, 2004; Jaqaman et al., 2010). All siRNA oligos were purchased from Dharmacon Research. The sequences for the p31^{comet} siRNA duplexes are p31^{comet}-1 (GGAGUUCUAUGAACUGGAC) and p31^{comet}-3 (CUGUAAUCAUCGCUGAACA). Duplexes and RNAi for Lamin A (Elbashir *et al.*, 2001), Mad1 and Mad2 (Martin-Lluesma et al., 2002) and hNuf2R (Meraldi et al., 2004) have been described. HeLa cells were transfected with siRNA as described (Elbashir *et al.*, 2001) and analyzed 48 hours after transfection. GFP-p31^{comet} and GFP-Mad2 were transiently expressed in HeLa Histone 2B-mRFP cells using Fugene 6 (Roche Diagnostics) and cells analyzed 16 hours after transfection.

In synchrony-release experiments that maximize protein depletion two of six tested anti-p31^{comet} siRNA oligos resulted in ~90-95% protein depletion as judged by immunoblotting and immunofluorescence using polyclonal anti-p31 antibodies (See Supplemental Figure 1). In contrast, transfection of cells with siRNA directed against Lamin A, a well-studied control for mitotic timing experiments, caused no changes in p31^{comet} levels.

Antibody dilutions for immunoblotting, immunofluorescence, and immunoprecipitation are in Supplementary Table 1. Polyclonal antibodies were raised in NZW rabbits against human p31^{comet} residues 1-138 expressed in *E. coli* (Covance). A column of immobilized p31^{comet} (1-138) was made with the SulfoLink kit (Pierce) for affinity purification of immune sera. Whole cell extracts were prepared by boiling cells in 2x SDS sample buffer with 15% β-ME before SDS-PAGE and immunoblotting.

Microscopy

Cells were fixed, permeabilized and blocked as described (Kapoor *et al.*, 2000). Cross-adsorbed secondary antibodies were used (Molecular Probes). HeLa Images were acquired as described (Martinez-Exposito *et al.*, 1999) and kinetochore fluorescence intensities were calculated as described (Meraldi *et al.*, 2004) . Live cell imaging was performed in ΔT 0.15 mm-dishes (Bioptechs) in CO_2-independent medium (GibcoBRL) at 37°C. 0.2s exposures were acquired every 3 min for 6 hr using a 20x NA0.75 objective on a Nikon Applied Precision Deltavision microscope equipped with a Mercury 100W lamp, GFP-long pass filter set (for Histone 2B-GFP-Hela cells) or a Sedat filter set (to follow GFP-proteins in Histone 2B-Red-Hela cells; Chroma) and Coolsnap HQ camera. Point visitation was used to follow cells in multiple fields. For measurements of inter-kinetochore distances EGFP–CENP-A cells were recorded live with a 100× 1.35 N.A. objective on an Olympus DeltaVision micro- scope (Applied Precision, LLC) equipped with a CoolSNAP HQ2 camera (Roper Scientific) and an EGFP

filter set (Chroma) at a temporal resolution of 7.5 s and the time-lapse images subjected to the kinetochore tracking assay analysis (Jaqaman *et al.*, 2010).

Mitotic frequency plots were generated as described (Meraldi *et al.*, 2004) . Anaphase entry half-lives were calculated by fitting cumulative frequency data from live cell imaging by nonlinear least squares regression in the nlintool of Matlab 7.0 (The Mathworks). Observed half-lives were considered to be the sum of the observed lag and the calculated $t_{1/2}$. The ratio of Mad1 or Mad2 levels versus CREST signal at kinetochores was determined as previously described (McAinsh *et al.*, 2006).

For FRAP and live PtK2 studies, imaging was carried out on Nikon TE-2000-E2 microscope equipped with an incubation chamber (in Vivo Scientifics) for environmental control, Photometrics COOLSNAP HQ cooled CCD camera and IPLab software (BD Biosciences) for microscope, camera and shutter-based acquisition. Fluorescence recovery (FRAP) experiments were carried out on the same microscopy system with the addition of a 3W argon-krypton laser tuned to 514 nm and attenuated to 10 mW at the back port of the microscope. The laser beam was expanded to slightly overfill the back aperture of a 60X high numerical aperture (NA = 1.4) objective. Laser exposure was restricted by a shutter (LUDL corporation) controlled by IPLab software and images were acquired after bleaching at 500 ms – 1 second intervals. Fluorescence recovery intensity measurements and curve fitting were carried out according to previously described methods (Shah *et al.*, 2004).

Mathematical Model

A mathematical model was constructed using published biochemical reactions, rate constants and affinities for Mad2-p31comet and APC/C-MCC interactions (Tables 1 and 2). All other rate constants were chosen based on qualitative affinities or rates that have been reported in the literature (Mapelli *et al.*, 2006; Vink *et al.*, 2006). While previous work has used a spatial model for simulations of checkpoint activity (Ciliberto and Shah, 2009), here we use a set of ordinary differential equations to represent the biochemical interactions produced at the kinetochore and that occur in the cytoplasm. The

scheme of the model has a set of reactions that have C-Mad2 in the context of Mad1 (Km2c) representing the kinetochore reactions.

$$m2o + Km2c \underset{\bar{k}_{mm}}{\overset{k_{mm}}{\rightleftarrows}} m2o{:}\,Km2c \xrightarrow{k_{mm}^{cat}} m2c + Km2c$$

$$p + Km2c \underset{\bar{k}_{pm}}{\overset{k_{pm}}{\rightleftarrows}} p{:}\,Km2c$$

$$a + m2c \underset{\bar{c}_{am}}{\overset{c_{am}}{\rightleftarrows}} m2c{:}\,a$$

$$m2o + m2c \underset{\bar{c}_{mm}}{\overset{c_{mm}}{\rightleftarrows}} m2o{:}\,m2c \xrightarrow{c_{mm}^{cat}} m2c + m2c$$

$$m2o + m2c{:}\,a \underset{\bar{c}_{mm}}{\overset{c_{mm}}{\rightleftarrows}} m2o{:}\,m2c{:}\,a \xrightarrow{c_{mm}^{cat}} m2c + m2c{:}\,a$$

$$p + m2c \underset{\bar{c}_{pm}}{\overset{c_{pm}}{\rightleftarrows}} p{:}\,m2c$$

$$\left.\begin{array}{l} p + a{:}\,m2c \underset{\bar{c}_{pm}}{\overset{c_{pm}}{\rightleftarrows}} \\ a + p{:}\,m2c \underset{\bar{c}_{am}}{\overset{c_{am}}{\rightleftarrows}} \end{array}\right\} p{:}\,m2c{:}\,a \xrightarrow{c_{pm}^{cat}} a + m2o + p$$

With m2o representing open Mad2, m2c – closed Mad2 (or MCC), Km2c – "kinetochore" Mad1-Mad2c, p – $p31^{comet}$, a – APC/C and ":" designates complex formation.

ACKNOWLEDGEMENTS

This work was supported by NIH grants CA084179 and GM51464 to P.K.S. and GM77238 to J.V.S.

REFERENCES

Chen, R.H., Shevchenko, A., Mann, M., and Murray, A.W. (1998). Spindle checkpoint protein Xmad1 recruits Xmad2 to unattached kinetochores. J Cell Biol *143*, 283-295.

Ciliberto, A., and Shah, J.V. (2009). A quantitative systems view of the spindle assembly checkpoint. Embo J *28*, 2162-2173.

De Antoni, A., Pearson, C.G., Cimini, D., Canman, J.C., Sala, V., Nezi, L., Mapelli, M., Sironi, L., Faretta, M., Salmon, E.D., and Musacchio, A. (2005). The Mad1/Mad2 complex as a template for Mad2 activation in the spindle assembly checkpoint. Curr Biol *15*, 214-225.

DeLuca, J.G., Howell, B.J., Canman, J.C., Hickey, J.M., Fang, G., and Salmon, E.D. (2003). Nuf2 and Hec1 are required for retention of the checkpoint proteins Mad1 and Mad2 to kinetochores. Curr Biol *13*, 2103-2109.

Elbashir, S.M., Harborth, J., Lendeckel, W., Yalcin, A., Weber, K., and Tuschl, T. (2001). Duplexes of 21-nucleotide RNAs mediate RNA interference in cultured mammalian cells. Nature *411*, 494-498.

Garnett, M.J., Mansfeld, J.o.r., Godwin, C., Matsusaka, T., Wu, J., Russell, P., Pines, J., and Venkitaraman, A.R. (2009). UBE2S elongates ubiquitin chains on APC/C substrates to promote mitotic exit. Nat Cell Biol *11*, 1363.

Habu, T., Kim, S.H., Weinstein, J., and Matsumoto, T. (2002). Identification of a MAD2-binding protein, CMT2, and its role in mitosis. Embo J *21*, 6419-6428.

Hardwick, K.G., Johnston, R.C., Smith, D.L., and Murray, A.W. (2000). MAD3 encodes a novel component of the spindle checkpoint which interacts with Bub3p, Cdc20p, and Mad2p. J Cell Biol *148*, 871-882.

Hardwick, K.G., Weiss, E., Luca, F.C., Winey, M., and Murray, A.W. (1996). Activation of the budding yeast spindle assembly checkpoint without mitotic spindle disruption. Science *273*, 953-956.

Hoffman, D.B., Pearson, C.G., Yen, T.J., Howell, B.J., and Salmon, E.D. (2001). Microtubule-dependent changes in assembly of microtubule motor proteins and mitotic spindle checkpoint proteins at PtK1 kinetochores. Mol Biol Cell *12*, 1995-2009.

Howell, B.J., Hoffman, D.B., Fang, G., Murray, A.W., and Salmon, E.D. (2000). Visualization of Mad2 dynamics at kinetochores, along spindle fibers, and at spindle poles in living cells. J Cell Biol *150*, 1233-1250.

Howell, B.J., Moree, B., Farrar, E.M., Stewart, S., Fang, G., and Salmon, E.D. (2004). Spindle checkpoint protein dynamics at kinetochores in living cells. Curr Biol *14*, 953-964.

Hoyt, M.A., Totis, L., and Roberts, B.T. (1991). S. cerevisiae genes required for cell cycle arrest in response to loss of microtubule function. Cell *66*, 507-517.

Jaqaman, K., King, E.M., Amaro, A.C., Winter, J.R., Dorn, J.F., Elliott, H.L., McHedlishvili, N., McClelland, S.E., Porter, I.M., Posch, M., Toso, A., Danuser, G., McAinsh, A.D., Meraldi, P., and Swedlow, J.R. (2010). Kinetochore alignment within the metaphase plate is regulated by centromere stiffness and microtubule depolymerases. The Journal of Cell Biology *188*, 665-679.

Kallio, M.J., Beardmore, V.A., Weinstein, J., and Gorbsky, G.J. (2002). Rapid microtubule-independent dynamics of Cdc20 at kinetochores and centrosomes in mammalian cells. J Cell Biol *158*, 841-847.

Kapoor, T.M., Mayer, T.U., Coughlin, M.L., and Mitchison, T.J. (2000). Probing spindle assembly mechanisms with monastrol, a small molecule inhibitor of the mitotic kinesin, Eg5. J Cell Biol *150*, 975-988.

Kulukian, A., Han, J., and Cleveland, D. (2009). Unattached Kinetochores Catalyze Production of an Anaphase Inhibitor that Requires a Mad2 Template to Prime Cdc20 for BubR1 Binding. Dev Cell *16*, 105-117.

Li, R., and Murray, A.W. (1991). Feedback control of mitosis in budding yeast. Cell *66*, 519-531.

Luo, X., Tang, Z., Xia, G., Wassmann, K., Matsumoto, T., Rizo, J., and Yu, H. (2004). The Mad2 spindle checkpoint protein has two distinct natively folded states. Nat Struct Mol Biol *11*, 338-345.

Mapelli, M., Filipp, F.V., Rancati, G., Massimiliano, L., Nezi, L., Stier, G., Hagan, R.S., Confalonieri, S., Piatti, S., Sattler, M., and Musacchio, A. (2006). Determinants of conformational dimerization of Mad2 and its inhibition by p31comet. Embo J *25*, 1273-1284.

Mapelli, M., Massimiliano, L., Santaguida, S., and Musacchio, A. (2007). The mad2 conformational dimer: structure and implications for the spindle assembly checkpoint. Cell *131*, 730-743.

Martinez-Exposito, M.J., Kaplan, K.B., Copeland, J., and Sorger, P.K. (1999). Retention of the BUB3 checkpoint protein on lagging chromosomes. Proc Natl Acad Sci USA *96*, 8493-8498.

McAinsh, A.D., Meraldi, P., Draviam, V.M., Toso, A., and Sorger, P.K. (2006). The human kinetochore proteins Nnf1R and Mcm21R are required for accurate chromosome segregation. Embo J *25*, 4033-4049.

Meraldi, P., Draviam, V.M., and Sorger, P.K. (2004). Timing and checkpoints in the regulation of mitotic progression. Dev Cell *7*, 45-60.

Musacchio, A., and Salmon, E.D. (2007). The spindle-assembly checkpoint in space and time. Nat Rev Mol Cell Biol *8*, 379-393.

Reddy, S.K., Rape, M., Margansky, W.A., and Kirschner, M.W. (2007). Ubiquitination by the anaphase-promoting complex drives spindle checkpoint inactivation. Nature *446*, 921-925.

Shah, J.V., Botvinick, E., Bonday, Z., Furnari, F., Berns, M., and Cleveland, D.W. (2004). Dynamics of centromere and kinetochore proteins; implications for checkpoint signaling and silencing. Curr Biol *14*, 942-952.

Shelby, R.D., Hahn, K.M., and Sullivan, K.F. (1996). Dynamic elastic behavior of alpha-satellite DNA domains visualized in situ in living human cells. J Cell Biol *135*, 545-557.

Simonetta, M., Manzoni, R., Mosca, R., Mapelli, M., Massimiliano, L., Vink, M., Novak, B., Musacchio, A., and Ciliberto, A. (2009). The influence of catalysis on mad2 activation dynamics. Plos Biol *7*, e10.

Sotillo, R., Hernando, E., Diaz-Rodriguez, E., Teruya-Feldstein, J., Cordon-Cardo, C., Lowe, S.W., and Benezra, R. (2007). Mad2 overexpression promotes aneuploidy and tumorigenesis in mice. Cancer Cell *11*, 9-23.

Sudakin, V., Chan, G.K., and Yen, T.J. (2001). Checkpoint inhibition of the APC/C in HeLa cells is mediated by a complex of BUBR1, BUB3, CDC20, and MAD2. J Cell Biol *154*, 925-936.

Teichner, A., Eytan, E., Sitry-Shevah, D., Miniowitz-Shemtov, S., Dumin, E., Gromis, J., and Hershko, A. (2011). p31comet promotes disassembly of the mitotic checkpoint complex in an ATP-dependent process. Proceedings of the National Academy of Sciences, 1-6.

Vigneron, S., Prieto, S., Bernis, C., Labbe, J.C., Castro, A., and Lorca, T. (2004). Kinetochore localization of spindle checkpoint proteins: who controls whom? Mol Biol Cell *15*, 4584-4596.

Vink, M., Simonetta, M., Transidico, P., Ferrari, K., Mapelli, M., De Antoni, A., Massimiliano, L., Ciliberto, A., Faretta, M., Salmon, E.D., and Musacchio, A. (2006). In vitro FRAP identifies the minimal requirements for Mad2 kinetochore dynamics. Curr Biol *16*, 755-766.

Williamson, A., Wickliffe, K.E., Mellone, B.G., Song, L., Karpen, G.H., and Rape, M. (2009). Identification of a physiological E2 module for the human anaphase-promoting complex. Proc Natl Acad Sci USA *106*, 18213-18218.

Wu, T., Merbl, Y., Huo, Y., Gallop, J.L., Tzur, A., and Kirschner, M.W. (2010). UBE2S drives elongation of K11-linked ubiquitin chains by the anaphase-promoting complex. Proc Natl Acad Sci USA *107*, 1355-1360.

Xia, G., Luo, X., Habu, T., Rizo, J., Matsumoto, T., and Yu, H. (2004). Conformation-specific binding of p31(comet) antagonizes the function of Mad2 in the spindle checkpoint. Embo J *23*, 3133-3143.

Yang, M., Li, B., Liu, C.-J., Tomchick, D.R., Machius, M., Rizo, J., Yu, H., and Luo, X. (2008). Insights into Mad2 Regulation in the Spindle Checkpoint Revealed by the Crystal Structure of the Symmetric Mad2 Dimer. Plos Biol *6*, e50.

Yang, M., Li, B., Tomchick, D.R., Machius, M., Rizo, J., Yu, H., and Luo, X. (2007). p31(comet) Blocks Mad2 Activation through Structural Mimicry. Cell *131*, 744-755.

Figure Legends

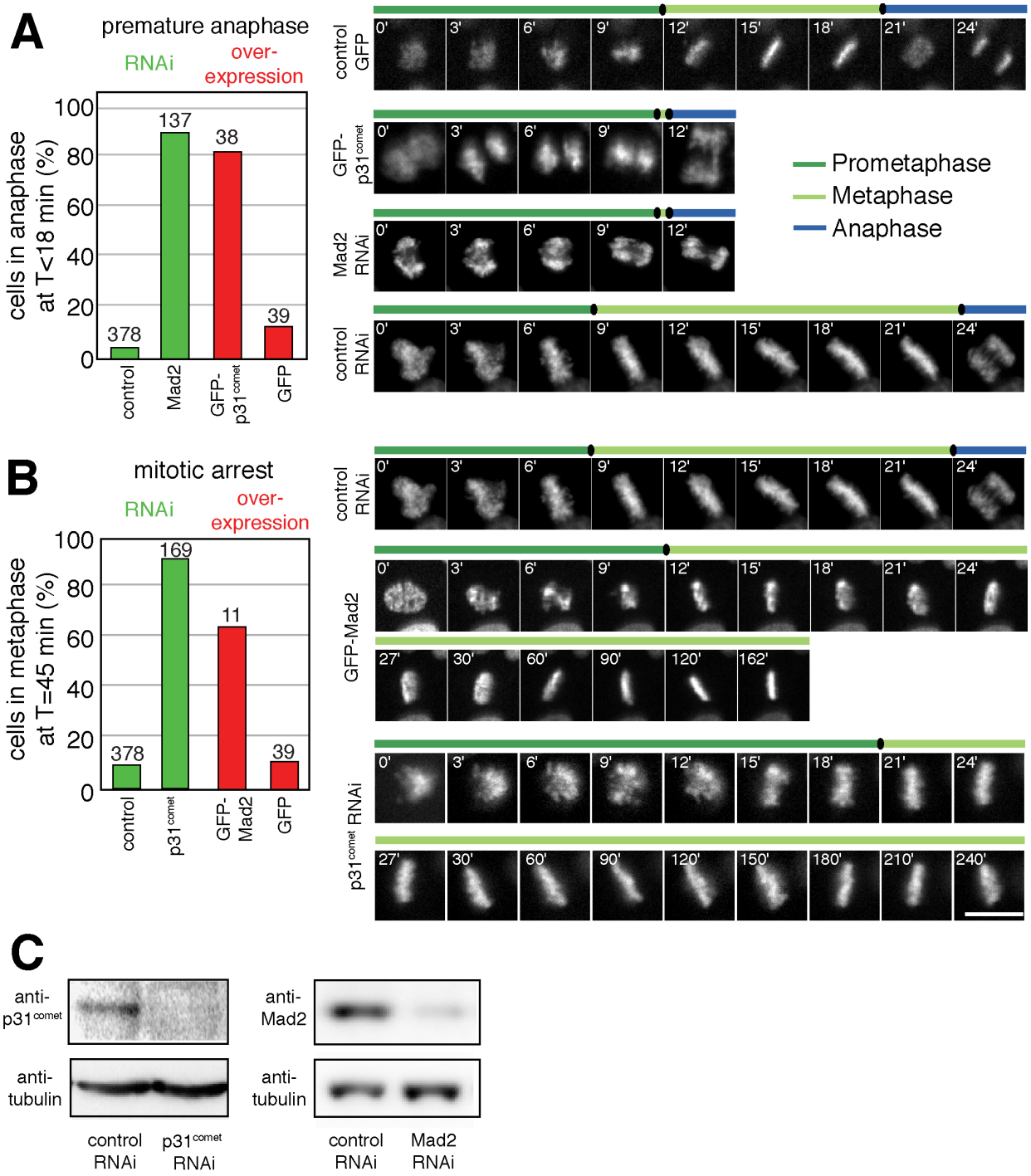

Figure 1

<u>p31^{comet} and Mad2 act in opposition to promote anaphase onset</u>

(A) p31^{comet} over-expression and Mad2 depletion cause premature anaphase. HeLa Histone 2B-mRFP cells were transfected with GFP or GFP-p31^{comet} and HeLa Histone 2B-GFP were transfected with Mad2

siRNA or control siRNA and followed by time-lapse microscopy. The times represent minutes after NBD; scale bar, 10 μm. The graph shows the fraction of cells undergoing premature anaphase, defined as chromosome segregation at T<18min. **(B)** $p31^{comet}$ depletion and Mad2 overexpression arrest cells in mitosis. As in (A), HeLa Histone 2B-GFP cells were transfected with $p31^{comet}$ or control siRNA and HeLa Histone 2B-mRFP cells were transfected with GFP-Mad2. The graph depicts fraction of cells arrested in mitosis, defined as still in metaphase at T>45min. **(C)** Immunoblots of whole cell lysates from HeLa cells treated with siRNA against lamin A (negative control), $p31^{comet}$, or Mad2. Blots were probed with antibodies as indicated.

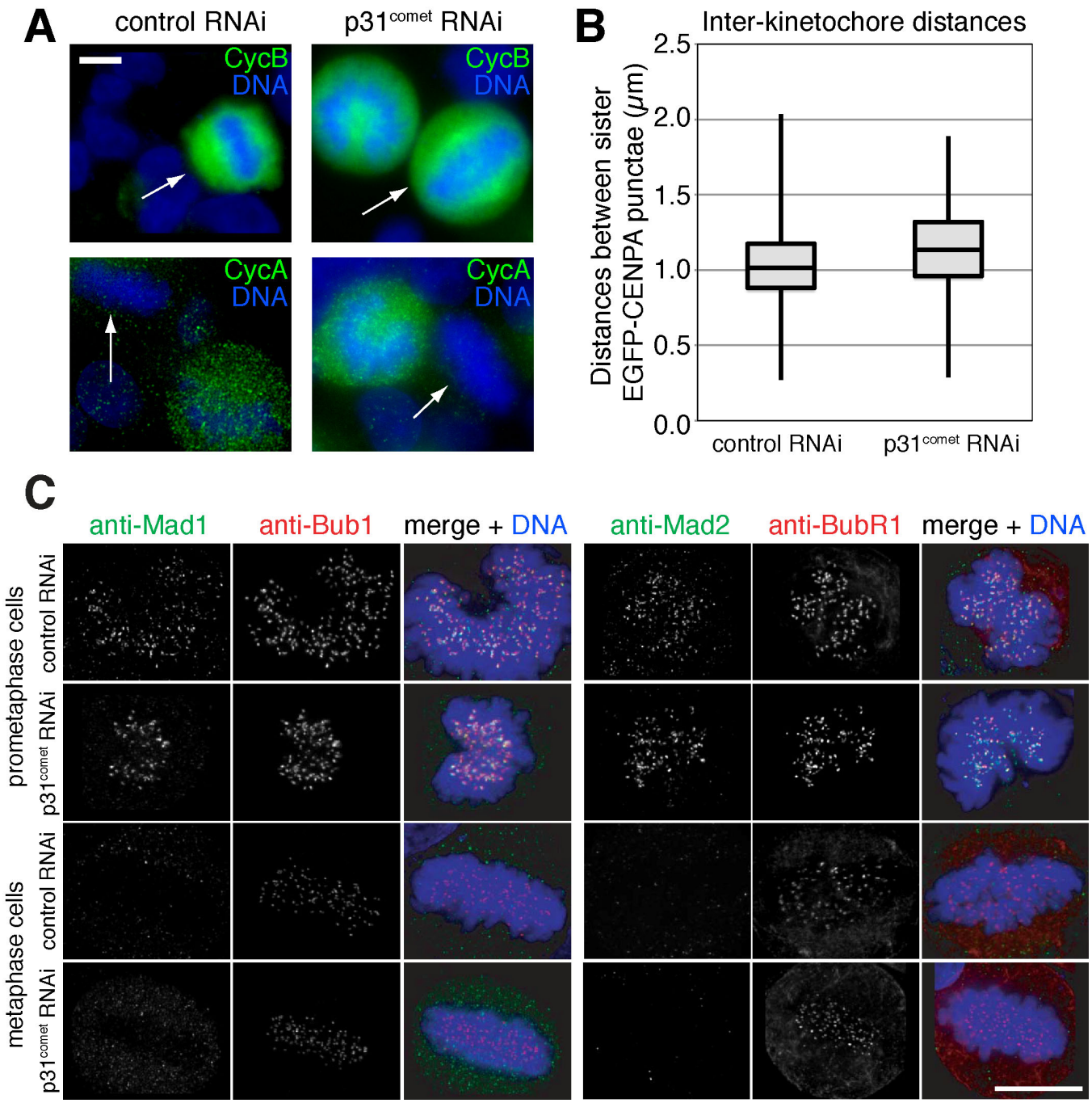

Figure 2

Cell cycle arrest following p31^{comet} depletion is not due to defective kinetochore-MT attachments or sustained kinetochore signaling

(A) Cells depleted of p31^{comet} arrest in mitosis. HeLa cells were treated with control or p31^{comet} siRNA and stained with DAPI (blue) and anti-cyclin B or anti-cyclin A (green). **(B)** Kinetochores in p31^{comet}-depleted cells are under tension. HeLa EGFP-CENP-A cells were transfected with siRNAs against

p31^{comet} or a control and interkinetochore distances were measured in metaphase cells using a kinetochore tracking assay. Interkinetochore distances are represented as Whisker plots based on 240 (p31^{comet}) and 319 (control) sister-kinetochore pairs in 2 independent experiments. **(C)** Checkpoint proteins localize normally in p31^{comet}-depleted cells. HeLa cells depleted for p31^{comet} or Lamin A control were stained with DAPI (blue) and antibodies against the indicated checkpoint proteins (red and green). Scale bars are 10μm.

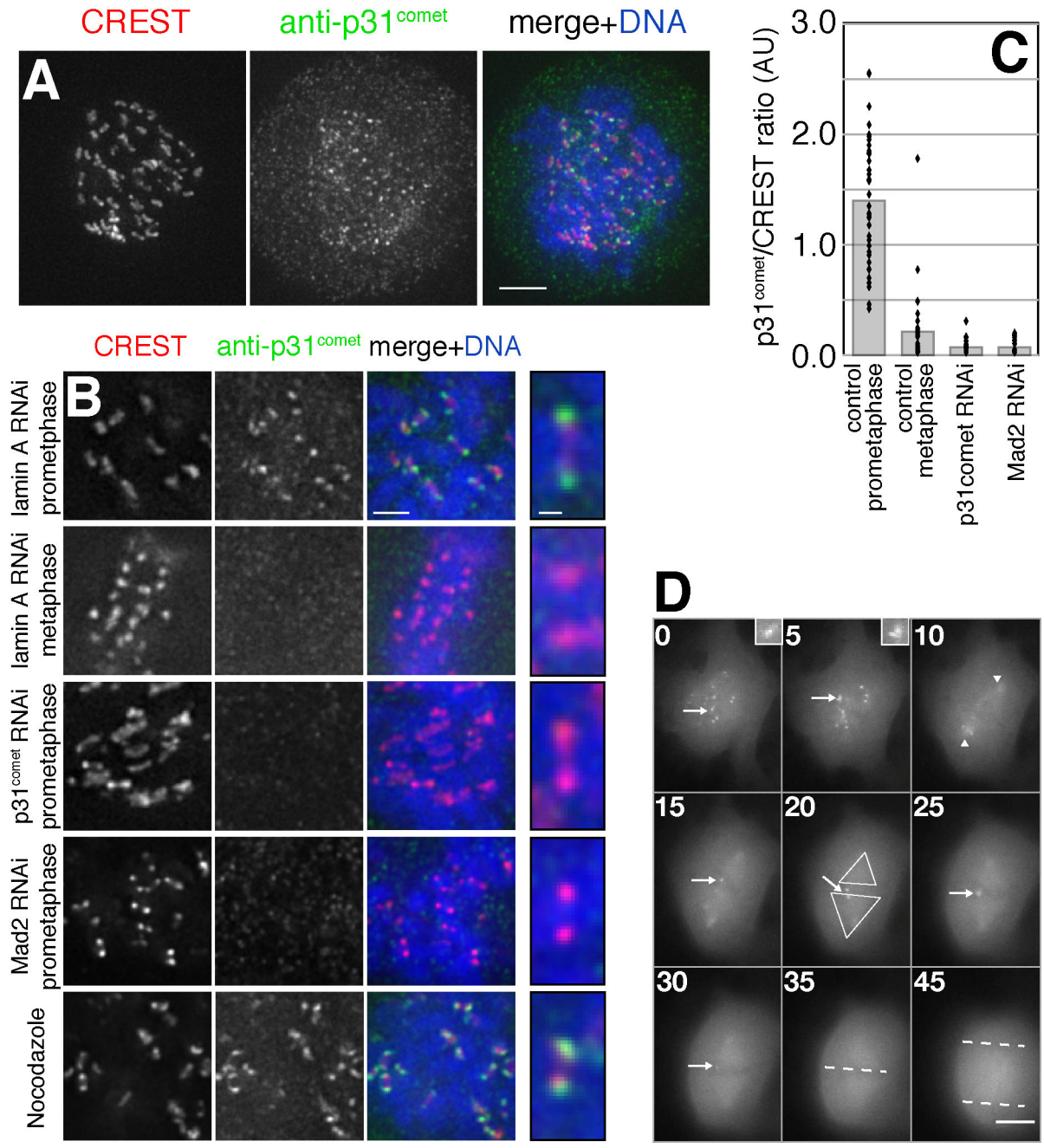

Figure 3

p31^{comet} localizes to unattached kinetochores in a Mad2-dependent fashion

(A) p31^{comet} localizes to unattached kinetochores. HeLa cells were stained with DAPI, anti-p31^{comet} antibodies, and CREST serum. Scale bar is 5µm. **(B)** p31^{comet} binds to kinetochores in prometaphase and requires Mad2. HeLa cells treated with the indicated siRNA were stained with DAPI, CREST, and anti-p31^{comet} antiserum. Scale bar is 2.5µm. Indicated sister kinetochore pairs are magnified at right;

scale bar is 0.5μm. **(C)** Quantitation of $p31^{comet}$ loss from kinetochores. $p31^{comet}$ /CREST signal ratios from individual kinetochores are plotted as dots; bars represent mean ratio values. **(D)** Images captured from a time-lapse sequence showing p31comet-EYFP localization during mitosis. Kinetochore localization (arrows) is most apparent in early prometaphase when chromosomes are unattached. Upon attachment a portion of the fluorescence is accumulates at spindle poles (arrowheads) and in the spindle region (triangles). After all chromosomes no longer have kinetochore accumulation, anaphase onset begins (dashed lines mark chromosome masses). Time points are in minutes. Scale bar represents 10μm.

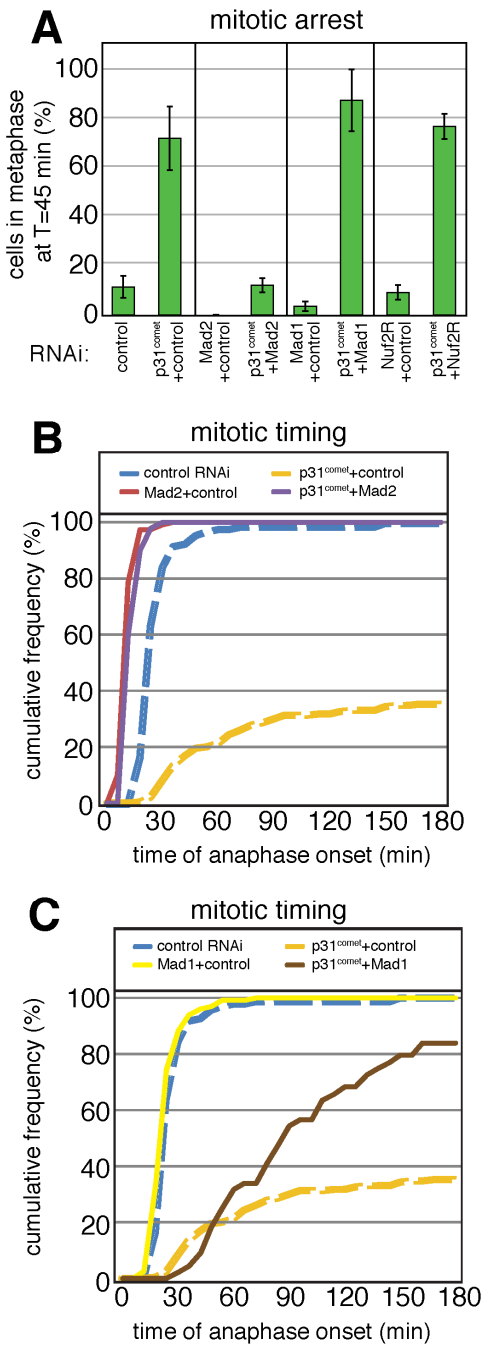

Figure 4

p31^{comet} acts downstream of the timer functions of Mad2 but upstream of kinetochore functions

(A) Mitotic arrest of HeLa Histone 2B-GFP cells was measured as in Fig 1B. Bars indicate mean and range of at least two independent experiments. **(B, C)** Cumulative frequency graphs of anaphase times in cells treated with siRNA as indicated. Dashed lines for control RNAi and p31^{comet}/control RNAi are identical between B and C.

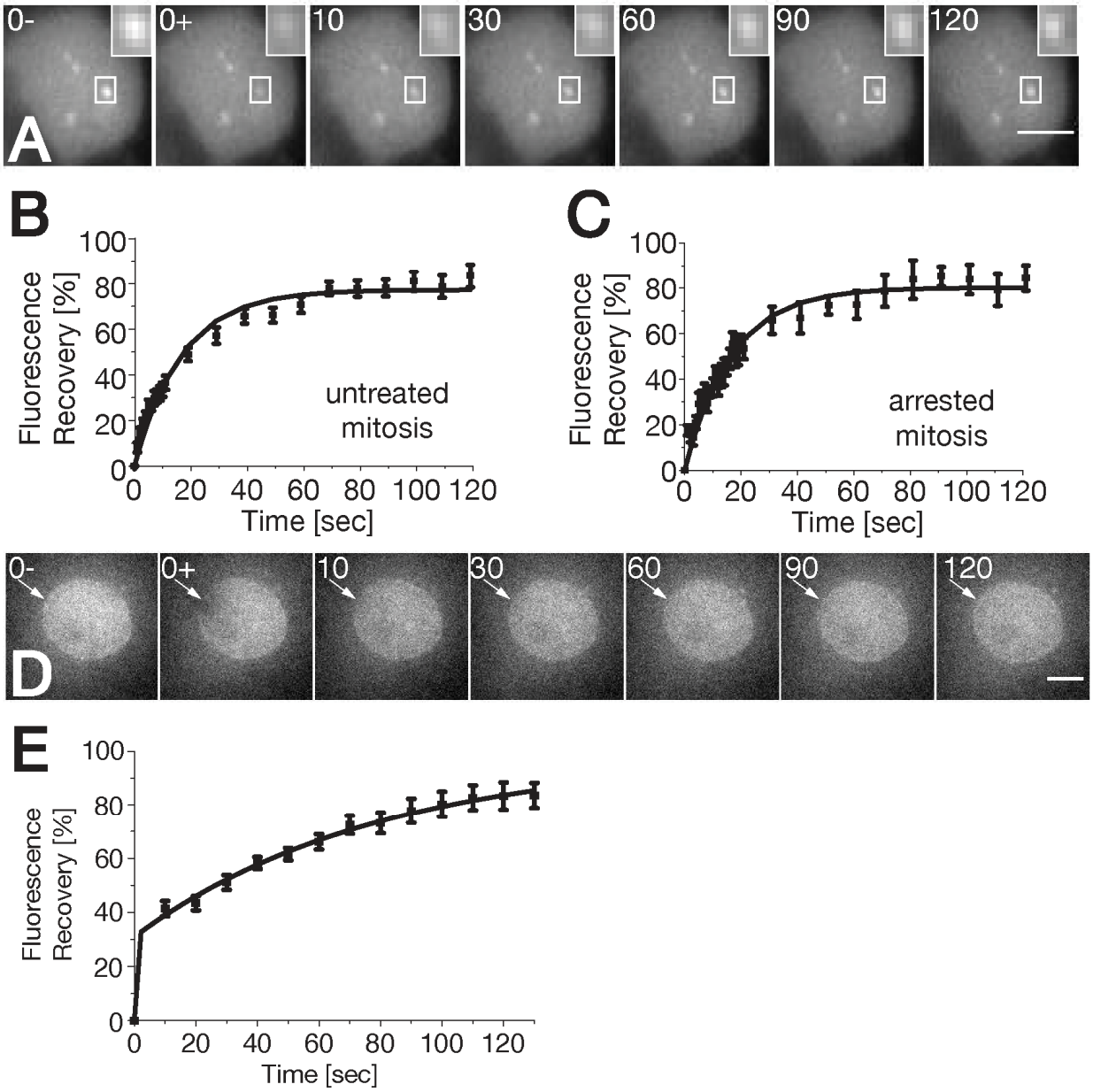

Figure 5

Trafficking of p31^{comet} on and off kinetochores

(A) An image sequence showing fluorescence recovery of p31^{comet}-EYFP after photobleaching at an unattached kinetochore. The inset shows the bleached kinetochore recovering in detail. Time points are in seconds. The scale bar represents 10µm. **(B)** Recovery curve for p31^{comet}-EYFP at unattached kinetochores in untreated PtK2 cells. **(C)** Recovery curve for p31comet-EYFP at unattached kinetochores in nocodazole-arrested PtK2 cells. **(D)** An image sequence showing fluorescence recovery of p31^{comet}-EYFP after photobleaching in the nucleoplasm and nuclear envelope. Time points are in

seconds. Scale bar is 5 μm. **(E)** Recovery curve for p31^{comet}-EYFP at the nuclear envelope in PtK2 cells shown as a percentage of the original fluorescence intensity over time. A biphasic curve had the best fit to the data. The fast phase is the diffusible nucleoplasmic fraction of p31^{comet}-EYFP whereas the slow fraction is p31^{comet} at the nuclear envelope.

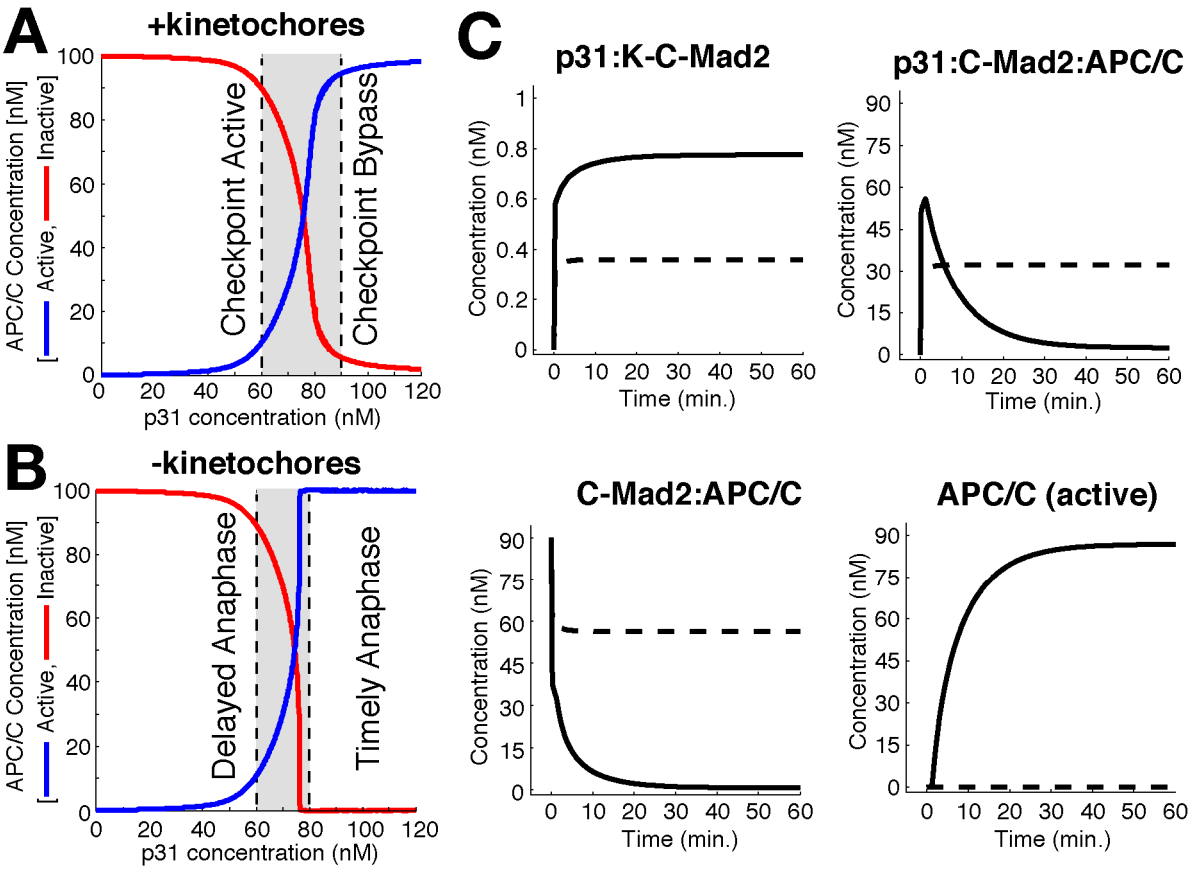

Figure 6

Computer-driven simulations demonstrating that p31^{comet} levels can control APC/C activity.

APC/C activation state as a function of active p31^{comet} concentration in the presence **(A)** or absence **(B)** of kinetochore signaling reveals a dependence of p31^{comet} on APC/C activation. **(C)** Checkpoint protein complexes dynamics are shown for two concentrations of p31^{comet}. The dashed line illustrates the addition of a low (50 nM) concentration of p31comet and the solid line, the addition of p31^{comet} to a high level (100 nM). The high levels of p31^{comet} result in a rapid 80% inhibition of the kinetochore pool (1 nM K-C-Mad2 present) but much lower (40%) in the lower p31^{comet} simulation. Through the combined action of C-Mad2 binding and C-Mad2-APC dissociation, the APC/C is partitioned between two interconverting inactive pools of p31:C-Mad2:APC/C and C-Mad2:APC/C. The result is that the APC/C is rapidly activated at the high p31^{comet} level, whereas it is inactive at the low level.

Supplemental Figure 1

Characterization of RNA interference for p31^{comet}

(A) RNAi depletion of p31^{comet}. Immunoblots of whole cell lysates from HeLa cells treated with siRNA against lamin A (negative control) or 2 siRNA duplexes against p31^{comet} were probed with antibodies as indicated. **(B)** Loss of p31^{comet} from kinetochores after p31^{comet} RNAi with multiple siRNA duplexes. HeLa cells were transfected with p31^{comet} -1, p31^{comet} -3, or control siRNA, fixed, and stained for p31^{comet}, Bub1, and DNA as in Figure 3. 4. p31^{comet} colocalizes with Bub1 in prometaphase.

Supplemental Figure 2

Quantification of Mad1 and Mad2 proteins in p31^{comet} RNAi

(A) HeLa cells transfected with control or p31comet siRNA were fixed and stained with antibodies for Mad1 or Mad2 and CREST and DAPI as shown. Scale bar = 10 microns **(B)** Co-staining of Mad1 and Mad2 with CREST permits the detailed quantification for Mad1 and Mad2 relative to CREST. Abundances were normalized to the checkpoint proteins levels in control prometaphase cells. This analysis shows that there are undetectable levels of Mad1 and Mad2 in metaphase cells silenced for p31^{comet}, similar to control RNAi cells. The mitotic stage was determined by DNA morphology. Error bars are s.e.m. Results are based on 2 independent experiments with 5 cells and 10 kinetochores/cell in each experiment.

Supplemental Figure 3

Localization of checkpoint proteins in p31^{comet} RNAi

(A) HeLa cells transfected with control or p31comet siRNA were fixed and stained with antibodies for checkpoint proteins as shown. **(B)** A summary of of checkpoint proteins abundance summarizing Figure 2, Figure 3, and this figure.

Supplemental Movie 1

Live cell microscopy of p31comet-EYFP in PtK2 cells

Tables

Species	Concentration	Initial condition
Total Mad2 (m2c, m2o)	120 nM	all Mad2-O
Kinetochore (Km2c)	1 nM	constitutive
$p31^{comet}$ (p)	adjusted	0 nM
APC/C (a)	90 nM	active APC/C

Table 1: Species concentrations used in simulations.

Rate Constant	Value	Units	Reference
k_{mm}	1	$nM^{-1}s^{-1}$	(Vink *et al.*, 2006)
k_{mm}^{cat}	0.25	s^{-1}	Estimated from (Howell *et al.*, 2000; Shah *et al.*, 2004; Simonetta *et al.*, 2009)
$\overline{k}_{mm}$	1000	s^{-1}	(Vink *et al.*, 2006)
k_{pm}	1	$nM^{-1}s^{-1}$	(Vink *et al.*, 2006)
$\overline{k}_{pm}$	25	s^{-1}	(Vink *et al.*, 2006)
c_{am}	1	$nM^{-1}s^{-1}$	(MSM, JVS, unpublished data)
$\overline{c}_{am}$	0.0001	s^{-1}	(MSM, JVS, unpublished data)
c_{mm}	1	$nM^{-1}s^{-1}$	(Vink *et al.*, 2006)
c_{mm}^{cat}	0.25	s^{-1}	(Simonetta *et al.*, 2009)
$\overline{c}_{mm}$	1000	s^{-1}	(Vink *et al.*, 2006)
c_{pm}	1	$nM^{-1}s^{-1}$	(Vink *et al.*, 2006)
c_{pm}^{cat}	0.01	s^{-1}	Estimated from (Reddy *et al.*, 2007)
$\overline{c}_{pm}$	25	s^{-1}	(Vink *et al.*, 2006)

Table 2: Rate constants used in simulations.